Various scenarios for transition to thorium fuel cycle in the single-fluid double-zone thorium molten salt reactor (SD-TMSR)

O. Ashraf[a,b,*], Andrei Rykhlevskii[c], G. V. Tikhomirov[a], Kathryn D. Huff[c]

[a] *Dept. of Theoretical and Experimental Physics of Nuclear Reactors, Institute of Nuclear Physics and Engineering, National Research Nuclear University MEPhI, 31, Kashirskoe Shosse, Moscow, 115409, Russian Federation*
[b] *Physics Department, Faculty of Education, Ain Shams University, Cairo, Egypt, 11341*
[c] *Dept. of Nuclear, Plasma, and Radiological Engineering, University of Illinois at Urbana-Champaign, Urbana, IL 61801, United States*

Abstract

Liquid-fueled Molten Salt Reactor (MSR) systems represent advances in safety, economics, sustainability, and proliferation resistance. The MSR has been designed to operate in Th/^{233}U fuel cycle with ^{233}U used as startup fissile material. Since ^{233}U does not exist in nature, We must examine other available fissile materials. This work investigates the fuel cycle and neutronics performance of the Single-fluid Double-zone Thorium-based Molten Salt Reactor (SD-TMSR) with different fissile material loadings at startup: low-enriched uranium (LEU) (19.79%), Pu mixed with LEU (19.79%), reactor-grade Pu (a mixture of Pu isotopes chemically extracted from Pressurized Water Reactor (PWR) spent nuclear fuel (SNF) with 33 GWd/tHM burnup), transuranic elements (TRU) from Light Water Reactor (LWR) SNF, and ^{233}U. The MSR burnup routine provided by SERPENT-2 is used to simulate the online reprocessing and refueling in the SD-TMSR. The effective multiplication factor, fuel salt composition evolution, and net production of ^{233}U are studied in the present work. Additionally, the neutron spectrum shift during the reactor operation is calculated. The results show that the continuous flow of reactor-grade Pu helps transition to the thorium

*Corresponding Author
Email address: osama.ashraf@edu.asu.edu.eg oabdelaziz@mephi.ru (O. Ashraf)

fuel cycle within a relatively short time ($\approx$ 4.5 years) compared to 26 years for ^{233}U startup fuel. Finally, using TRU as initial fissile materials offers the possibility of operating the SD-TMSR for an extended period of time ($\approx$ 40 years) without any external feed of ^{233}U.

Keywords: MSR, thorium fuel cycle, transmuter, burner, online reprocessing, Monte carlo code

1. Introduction

The Generation IV International Forum (GIF) defines eight technological goals for the next generation nuclear systems. These goals are defined in four broad areas: safety and reliability, non-proliferation and physical protection, economics, and sustainability [1]. The Molten Salt Reactor (MSR) has many advantages that agree with GIF's goals, like: liquid fuel, inherent safety, online reprocessing and refueling, excellent neutron economy, and operation near atmospheric pressure in a primary loop [2, 3]. Thus, the GIF selected the MSR as one of the promising Generation-IV reactors [1, 4]. In the MSR, the fuel is dissolved in a molten salt (e.g., LiF or NaCl); this liquid fuel salt (e.g., LiF-BeF_2-ThF_4-$^{233}UF_4$) constantly circulates through the core and allows fission heat to transfer from the reactor core to intermediate heat exchangers.

The Single-fluid Double-zone Thorium-based Molten Salt Reactor (SD-TMSR) 2,250 MW_{th} was introduced by the Chinese Academy of Sciences [5]. The SD-TMSR is a graphite-moderated thermal-spectrum MSR operating in Th/^{233}U fuel cycle. In the SD-TMSR the fissile and fertile elements are integrated into the same salt. The active core is divided into two zones; the radius of the fuel channels in the outer zone is modified to be larger than the radius of the fuel channels in the inner zone to improve the breeding ratio [6, 5].

Historically, the thermal-spectrum MSR was designed for the Th/^{233}U fuel cycle [7, 6, 8, 3]. This design assumes that we have fissile ^{233}U inventory to start up new MSRs. However, ^{233}U does not exist in the Earth's crust and can only be produced from fertile ^{232}Th in specific nuclear facilities. Therefore, we examine

alternative fissile materials to replace the ^{233}U in the startup fuel composition [9, 10]. The thorium fuel cycle transition can be achieved after reaching the doubling time[1] of ^{233}U because in this case, all startup fissile material is being substituted by newly produced ^{233}U.

Betzler *et al.* (2016) discussed the simulation of the startup of a Molten Salt Breeder Reactor (MSBR) unit cell with low-enriched uranium (LEU) (19.79%) and Pu from Light Water Reactor (LWR) spent nuclear fuel (SNF) as initial fissile materials [9]. They concluded that the Pu vector extracted from LWR SNF is the best alternative source to ^{233}U because it has a high ratio of fissile isotopes [9]. Zou *et al.* (2018) introduced two approaches for the thorium fuel cycle transition in the Thorium-based Molten Salt Reactor (TMSR): (1) in-core transition and (2) ex-core transition. In the first approach, the TMSR is launched with existing fissile material and thorium as a fertile material; then the ^{233}U bred from thorium is rerouted into the core to maintain criticality. In contrast, the second approach tends to store produced ^{233}U out of the core until there is enough to start a new TMSR [10]. Zou *et al.* (2018) studied the transitioning to thorium fuel cycle in a small modular Thorium-based Molten Salt Reactor (smTMSR) using transuranic elements (TRU) as startup fuel. They concluded that the transition to the thorium fuel cycle can be achieved in a thermal smTMSR with a proper fuel fraction [11].

Heuer *et al.* (2014) discussed the transition characteristics of the Molten Salt Fast Reactor (MSFR) under different launching scenarios (e.g., enriched uranium and TRU); they concluded that starting the thorium fuel cycle is feasible while closing the current fuel cycle and adopting stockpile incineration in MSRs for optimizing the long-term waste management [12].

There are various researches that revolve around starting the MSRs with fissile materials alternative to ^{233}U. Many of these researches focus on the fast-spectrum MSRs [12, 13, 14, 15, 16, 17], while few focus on thermal-spectrum MSRs [9, 10, 11]. Simulating the operation of the Single-fluid Double-zone

[1] Time required to produce enough amount of ^{233}U to trigger a new SD-TMSR.

Thorium-based Molten Salt Reactor (SD-TMSR) concept with other fissile materials (except ^{233}U) has not been studied before. Therefore, the main objective of the present paper is to discuss the simulation of the SD-TMSR operation for a lifetime-long period of time (60 years) with different initial fissile materials and without any external feed of ^{233}U to achieve the thorium fuel cycle transition. We investigate five different initial fissile materials: LEU, Pu mixed with LEU, reactor-grade Pu, TRU from LWR SNF, and ^{233}U [18]. Two different feed mechanisms were selected:

- Thorium feed mechanism: continuous feed flow of thorium from the thorium stockpile and ^{233}U from the `Pa-decay tank`[2], where the removal rate of ^{233}Pa = feed rate of ^{233}U. [9].

- Non-thorium feed mechanism: continuous injection of heavy metal (excluding Th) and simultaneous feed of all or fraction of ^{233}U from the `Pa-decay tank`.

All calculations presented in this paper are performed using SERPENT-2 version 2.1.31 [19]. We use the MSR burnup routine provided by SERPENT-2 to simulate continuous online reprocessing and refueling. SERPENT-2 uses an internal calculation routine for solving the set of Bateman equations describing the changes in the material compositions caused by neutron-induced reactions and radioactive decay [19]. Additionally, SERPENT-2 allows us to conduct the burnup calculations on computer clusters with multiple cores using distributed-memory MPI parallelization.

This paper is organized as follows: section 1 introduces MSR systems, section 2 discusses the model description, section 3 describes methodology and tools, section 4 addresses extraction and feed mechanisms, section 5 focuses on the results and discussion, and section 6 highlights the conclusions.

[2] An imaginary tank used to store protactinium extracted from the core.

2. Model description

2.1. Geometry

The Single-fluid Double-zone Thorium-based Molten Salt Reactor (SD-TMSR) design model was introduced by the Chinese Academy of Sciences as a part of the strategic project "Future Advanced Nuclear Energy − Thorium-based Molten Salt Reactor System (TMSR)" in 2011 [5, 20, 21, 22]. The design of the SD-TMSR is inspired by the MSBR [23] after modifying the geometry to control the positive temperature coefficient in the MSBR. The SD-TMSR core geometry is described in detail by Li *et al.* [5]; Figure 1 illustrates the quarter-core model configuration of the SD-TMSR. The active zone is a right cylinder with height and diameter equal to 460 cm. Assemblies of graphite[3] hexagonal prisms fill the core. The optimal side length of the graphite hexagonal prism is found to be 7.5 cm [5]. The liquid fuel circulates continuously through the fuel channels that pierce the graphite hexagonal prisms. The core is divided into two different zones to enhance Th/^{233}U breeding performance; the radii of the fuel channels in the outer and inner zone are 5 and 3.5 cm, respectively. The axial and radial graphite reflectors surround the core to minimize neutron leakage and maximize flux in the core. The reflectors are surrounded by a B_4C cylinder that acts as radiation shielding. The SD-TMSR pressure vessel holds the fuel salt, graphite elements, reflector, shielding, intermediate heat exchanger, and is made of a Ni-based (hastelloy N) alloy. The main characteristics of the SD-TMSR are listed in Table 1.

2.2. Fuel composition

The general composition of the liquid fuel salt in this work is 70LiF - 17.5BeF_2 - 12.5(HM)F_4 mole%, where HM is the heavy metal (mixture of thorium and other actinides). The aim of this paper is to simulate the operation of SD-TMSR for 60 years with different startup fissile compositions and without any external

[3] We choose graphite density of 2.3 g/cm^3, to validate our results against results in literature [5, 6].

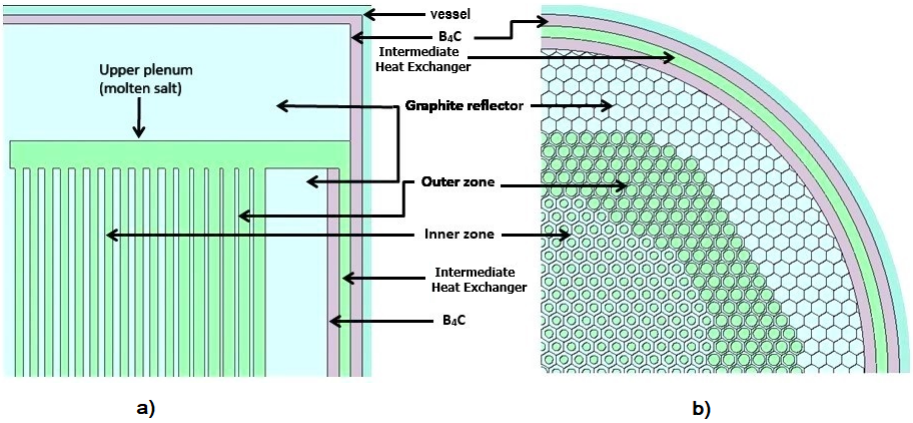

Figure 1: XZ (a) and XY (b) section of the quarter-core model of the SD-TMSR [24].

Table 1: The main characteristics of the SD-TMSR [5].

Thermal power, MW_{th}	2,250
Fuel salt components	LiF-BeF_2-$(HM)F_4$
Fuel composition, mole%	70-17.5-12.5
^{7}Li enrichment, %	99.995
Fuel temperature, K	900
Fuel density at 900 K, g/cm^3	3.3
Fuel dilatation coefficient, g/(cm^3.K)	-6.7×10^{-4}
Graphite density, g/cm^3	2.3
B_4C density, g/cm^3	2.52
^{10}B enrichment, %	18.4
Core diameter, cm	460
Core height, cm	460
Side length of the graphite hexagonal prism, cm	7.5
Inner radius, cm	3.5
Outer radius, cm	5
Ratio of molten salt and graphite in the inner zone	0.357
Ratio of molten salt and graphite in the outer zone	1.162
Fuel volume, m^3	52.9

Table 2: Reactor-grade Pu vector (wt.%) [25].

^{238}Pu	^{239}Pu	^{240}Pu	^{241}Pu	^{242}Pu
1.3	60.3	24.3	9.1	5

Table 3: TRU vector (wt.%) [18].

^{237}Np	^{238}Pu	^{239}Pu	^{240}Pu	^{241}Pu	^{242}Pu	^{241}Am	^{243}Am	^{244}Cm	^{245}Cm
6.3	2.7	45.9	21.5	10.7	6.7	3.4	1.9	0.8	0.1

feed of fissile ^{233}U which we assume is unavailable. For that reason, five different types of initial fissile materials are considered based on LEU, Pu, and TRU from Light Water Reactor (LWR) spent nuclear fuel (SNF):

(a) low-enriched uranium (LEU) (19.79%),

(b) Pu mixed with LEU (19.79%),

(c) reactor-grade Pu [25],

(d) transuranic (TRU) elements from LWR SNF [18], and

(e) ^{233}U for comparison [26].

The reactor-grade Pu and TRU compositions are summarized in Table 2 and 3, respectively.

For the reactor-grade Pu case, the composition is taken for Pu recovered from the SNF composition of a commercial Pressurized Water Reactor (PWR) with an average discharge burnup of 33 GWd/tHM and after 10 years of cooling before reprocessing [27, 25]. Similarly, the isotopic compositions of TRU are taken for the SNF of uranium oxide PWR (after one use, no multi-recycling) with an average discharge of 60 GWd/tHM burnup and after 5 years of cooling [18]. The molar composition of startup fuel for all five cases is listed in Table 4. Additionally, the corresponding initial nuclei inventories with different types of fuel are summarized in Table 5.

Table 4: Composition of startup fuel (mole%).

Fuel salt component	LEU (19.79%)	Pu+enriched U (19.79wt.%)	reactor-grade Pu	TRU	^{233}U
LiF	70	70	70	70	70
BeF_2	17.5	17.5	17.5	17.5	17.5
ThF_4	8.25	7.5	10.75	8.65	12.3
UF_4	4.25	4.75			0.2
PuF_3		0.25	1.75		
$(TRU)F_3$				3.85	

3. Methodology and tools

Simulation of liquid-fueled Molten Salt Reactor (MSR) systems requires computational software that must support online fuel salt reprocessing and refueling [28]. In this work, SERPENT-2 version 2.1.31 beta[4] [19] is used to simulate the full-core of the Single-fluid Double-zone Thorium-based Molten Salt Reactor (SD-TMSR) with different types of initial fuel. The extension of SERPENT accounts for continuous online reprocessing and refueling [29]. The ENDF-VII.0 cross section library was used for all calculations in this work. The results demonstrate full-core runs of 1.25×10^7 neutron histories per depletion step. The full burnup time of the SD-TMSR was 60 years with statistical error in k_{eff} equal to $\pm$ 12 *pcm*. The online extraction of fission products (FPs) and other neutron absorbers provides many benefits for MSRs. For example, it would reduce the initial fissile material inventory required to achieve criticality and improve the breeding ratio. Figure 2 shows a flow chart of the calculation steps.

As shown in Figure 2, after launching the input file, we solve the Bateman equation using an advanced matrix exponential solution based on the Chebyshev Rational Approximation Method [30]. Then, the system extracts gaseous FPs

[4]SERPENT-2 is a 3D continuous energy Monte Carlo neutron transport and burnup code.

Table 5: Initial heavy metal inventories for different initial fissile loadings (g).

Nuclide	LEU (19.79%)	Pu+enriched U (19.79wt.%)	reactor-grade Pu	TRU	^{233}U
^{232}Th	6.24E+07	4.67E+07	6.75E+07	5.44E+07	7.69E+07
^{233}U					1.30E+06
^{235}U	3.17E+06	6.01E+06			
^{238}U	1.28E+07	2.43E+07			
^{237}Np				1.58E+06	
^{238}Pu		1.60E+04	1.13E+05	6.78E+05	
^{239}Pu		9.59E+05	6.76E+06	1.15E+07	
^{240}Pu		3.99E+05	2.82E+06	5.40E+06	
^{241}Pu		1.60E+05	1.13E+06	2.69E+06	
^{242}Pu		6.39E+04	4.51E+05	1.68E+06	
^{241}Am				8.53E+05	
^{242}Am					
^{243}Am				4.77E+05	
^{244}Cm				2.01E+05	
^{245}Cm				2.51E+04	
Total*	1.60E+07	3.20E+07	1.13E+07	2.51E+07	1.30E+06

* Excluding ^{232}Th inventory.

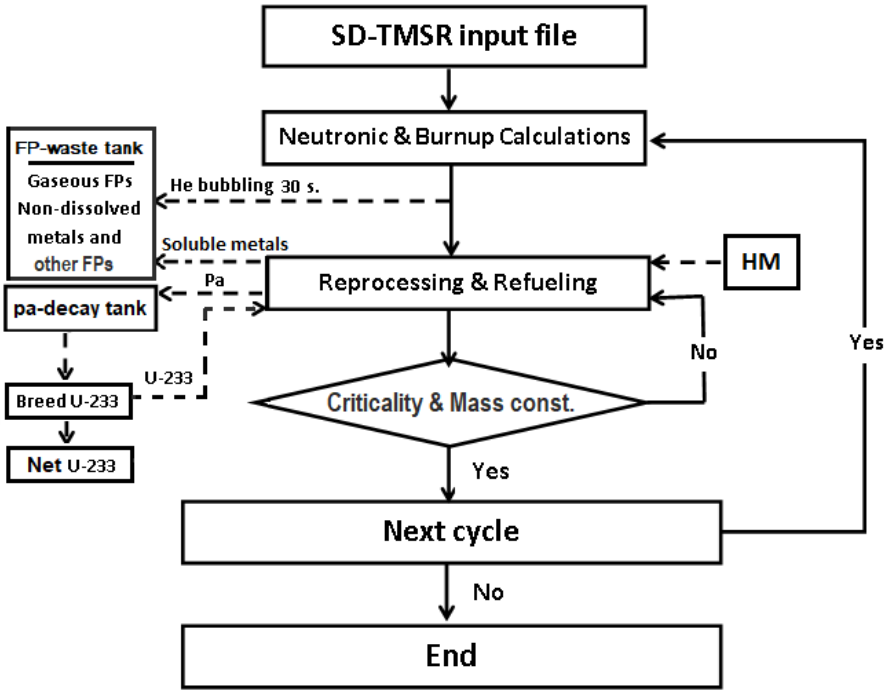

Figure 2: Flow chart of the calculation procedures.

and other materials (non-dissolved metals, lanthanides, and soluble metals except Pa) with a suitable removal rate[5]. This is done by setting the flow rate of gaseous FPs and other materials from the fuel to the `FP-waste tank`[6]. Specifically, Pa is removed from the fuel with a certain flow rate into the `Pa-decay tank` to decay and produce ^{233}U[7]. The produced ^{233}U is used as a fresh fissile fuel and the residual ^{233}U is the net production of ^{233}U. The MSR burnup routine provided by SERPENT-2 allows changes to the flow rates ($mflow$) of the isotopes during reactor operation [29]. Specifically, we have to determine the flow rate ($mflow$), which is the rate by which elements or nuclides are transferred between materials. After that, the flow rates must be connected to materials with a reprocessing

[5]The extraction rate depends on the type of poison and its impact on the neutron economy.

[6]An imaginary tank used to store the gaseous FPs and the other materials (non-dissolved metals, lanthanides, and soluble metals except protactinium).

[7]The ^{233}Pa is removed and left to decay into ^{233}U with $\tau_{1/2} \approx 27\ d$.

scheme. Finally, we have to link the reprocessing schemes to depletion histories. In the present work, we adjust the transfer rates of fresh fuel to maintain core criticality and to keep fuel salt inventory constant during burnup. The feed constant calculation procedures are summarized as follows:

1. The simulation starts without injecting refueling materials (i.e. only removing FPs and Pa).

2. After the first depletion calculation step, we check the total mass density of FPs and Pa in the `FP-waste tank` and `Pa-tank`, respectively.

3. A simple calculation yields the amount of heavy metal that must be added during this cycle:

   3a. For thorium feed mechanism: mass of Th $\approx$ mass of extracted FPs and mass of ^{233}U $\approx$ mass of extracted Pa.

   3b. For non-thorium feed mechanism: mass of the heavy metals (excluding Th) $\approx$ mass of extracted FPs and mass of ^{233}U $\approx$ mass of extracted Pa.

4. Dividing this mass by time and inventory of refueling material gives the corresponding feed constant.

The cycle calculation runs iteratively until the burnup reaches the desired worth.

4. Feed and extraction rates

In the present work, two different feed mechanisms are used: (1) thorium feed mechanism and (2) non-thorium feed mechanism. The first mechanism allows continuous feed flow of thorium from the thorium stockpile and ^{233}U from the `Pa-decay tank`. In contrast, the second mechanism continuously injects heavy metal (HM) (excluding Th) and simultaneously feeds all or part of produced ^{233}U from the `Pa-decay tank`. The fission products FPs act as poisons in the MSRs; they negatively impact the reactivity. Therefore, FPs must be extracted during reactor operation. Consider T_r as the time during which the total fuel

salt is reprocessed and dN_e as the amount of particular element e with inventory N_e that the MSR extracts during time dt; thus [6]

$$\frac{dN_e}{dt} = N_e \frac{\varepsilon_e}{T_r}, \tag{1}$$

where ε_e is the removal efficiency. Integration of equation 1 gives the removal constant λ_e $[s^{-1}]$ (the rate at which the material is removed), where $\lambda_e = \varepsilon_e / T_r$. The removal constant λ_e of gaseous and other fission products is precisely calculated and summarized in Table 6. The effective reprocessing time for the gaseous FPs and non-dissolved metals was set to 30 s (removal constant $\lambda_e = -0.0333\ s^{-1}$), because such elements must be extracted promptly and continuously via a gas removal system. In contrast, extracting the soluble FPs, lanthanides, and Pa is done by chemical reprocessing (i.e. fluorination and reduction reaction). Therefore, the system reprocesses a specific amount of fuel salt daily. In the present work, the effective extraction time for soluble FPs is ≈10.59 days ($\lambda_e = -1.092 \times 10^{-6}\ s^{-1}$), which is equivalent to a chemical reprocessing rate of 5 m^3/d [5, 6]. The effective feed rates of the heavy metals (HM) are changed during reactor operation to conserve the total fuel mass and criticality. The effective feed rates for Th/^{233}U, reactor-grade Pu, and TRU cases are listed in Table A.1, A.2, and A.3 in Appendix.

Table 6: The reprocessing table [26].

Reprocessing group	**Element**	**Reprocessing time**	**Removal constant λ_e $[s^{-1}]$**
Gaseous FPs and non-dissolved metals	H, He, N, O, Ne, Ar, Kr, Nb, Mo, Tc, Ru, Rh, Pd, Ag, Sb, Te, Xe, Lu, Hf, Ta, W, Re, Os, Ir, Pt, Au, and Rn.	30 s	-3.333E-02
Lanthanides and other soluble FPs	Zn, Ga, Ge, As, Se, Br, Rb, Sr, Y, Zr, Cd, In, Sn, I, Cs, Ba, La, Ce, Pr, Nd, Pm, Sm, Eu, Gd, Tb, Dy, Ho, Er, Tm, and Yb.	10.599 d (5 m^3/d)	-1.092E-06
Protactinium	Pa	10.599 d (5 m^3/d)	-1.092E-06

5. Results and discussion

5.1. Thorium feed mechanism

The thorium feed mechanism adopts continuous feed flow of external thorium from the thorium stockpile and ^{233}U from the `Pa-decay tank`. The molar fraction of the heavy metal in the initial fuel was kept constant and equal to 12.5 mole% for all cases. Additionally, the initial fissile material fraction was increased for the five fuel salt compositions until the SD-TMSR reactor was sufficiently critical at the Beginning Of Life (BOL). Figure 3 illustrates the effective multiplication factor dynamics during reactor operation for the thorium feed mechanism. As shown in Figure 3, the effective multiplication factor (k_{eff}) decreases sharply during the first 25 effective full-power years (EFPY) of reactor operation for the first four cases. k_{eff} decreases as a result of depletion of the initial fissile materials and production of poisonous fission products (FPs). Thus, the reactor becomes subcritical relatively quickly for alternative startup

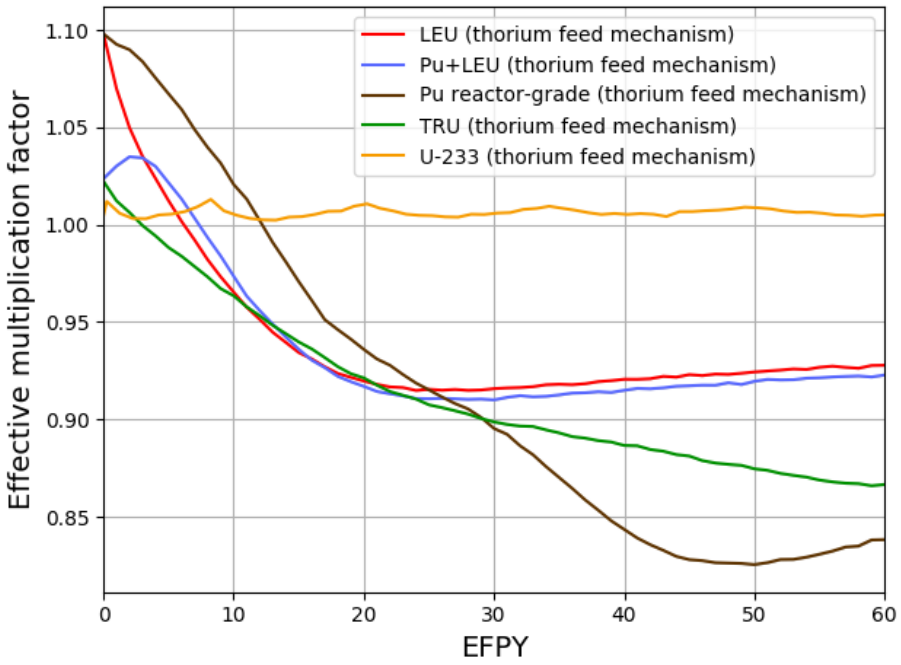

Figure 3: The change of the effective multiplication factor during 60 EFPY of reactor operation for thorium feed mechanism (confidence interval $\pm\sigma$ is shaded).

compositions, for example, $\approx$ 4 years in the TRU case and $\approx$ 12 years in the reactor-grade Pu case. The amount of ^{233}U generated in the Single-fluid Double-zone Thorium-based Molten Salt Reactor (SD-TMSR) is not enough to maintain the reactor criticality and counteract parasitic neutron absorption. Nevertheless, the continuous feed flow of thorium and ^{233}U helps to operate the SD-TMSR for a lifetime-long period of time (Figure 3 (U-233 case)). Additionally, the molar fraction of the LEU and reactor-grade Pu in the initial fuel composition was increased more, consequently, the initial k_{eff} for these cases increased (Figure 3 (LEU and reactor-grade Pu cases)). Nevertheless, k_{eff} still decreases below 1.0, as a result of increasing the non-fissile heavy metals in the initial fuel [9].

5.2. Non-thorium feed mechanism

The non-thorium feed mechanism allows continuous feed flow of ^{233}U from the `Pa-decay tank` and external heavy metals (excluding Th). Under the non-

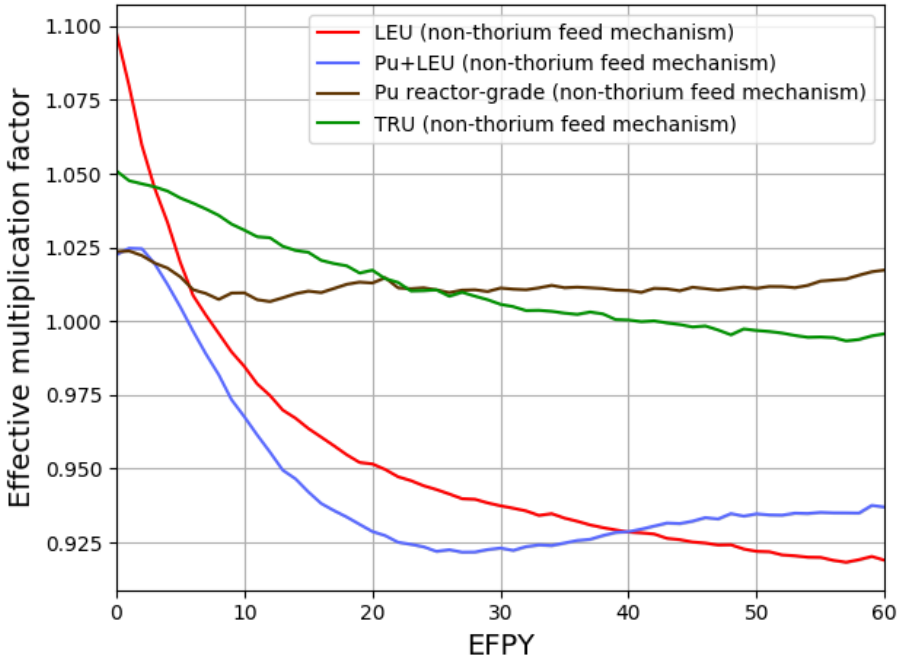

Figure 4: The change of the effective multiplication factor during 60 EFPY of reactor operation for non-thorium feed mechanism (confidence interval $\pm\sigma$ is shaded).

thorium feed mechanism, four different initial fissile materials are studied: LEU, Pu mixed with LEU, reactor-grade Pu, and TRU. The continuous feed of ^{233}U without ^{232}Th will lead to a supercritical reactor, thus the ^{233}U case is excluded from the non-thorium feed mechanism study. The molar fraction of the heavy metal in the initial fuel was kept constant and equal to 12.5 mole% for all cases. Additionally, the initial fissile material fraction was increased for the four fuel salt compositions until the SD-TMSR reactor was sufficiently critical at the BOL. Figure 4 shows the change of the effective multiplication factor during 60 EFPY of reactor operation for the non-thorium feed mechanism. Both the reactor-grade Pu and TRU cases show promising results relative to the other two cases (LEU and Pu+LEU) (see Figure 4).

For the reactor-grade Pu case, the amount of ^{233}U generated in the SD-TMSR, in addition to the external feed flow of Pu, is sufficient to maintain the reactor criticality and counteract the neutron absorption in the initial non-fissile

isotopes and FPs. For the TRU fuel salt, the amount of ^{233}U and the external feed flow of TRU is barely enough to operate the reactor for a long period of time ($\approx$ 40 years) without any external feed of ^{233}U (^{233}U used only from the `Pa-decay tank`). Nevertheless, k_{eff} decreases with the burnup because of the minor actinides (MAs)[8] accumulating in the core as a result of continuous TRU feed. As shown in Figure 4, the LEU and Pu+LEU fuel are less attractive for the non-thorium feed mechanism. The continuous LEU feed increases the amount of fertile ^{238}U and consequently, reduces the feasibility of such fissile materials. According to the k_{eff} results, reactor-grade Pu and TRU are the only alternative fissile materials that can be used to startup and maintain operation of the SD-TMSR.

5.3. Reactor-grade Pu, TRU, and ^{233}U initial fuel

In this section, the simulation of the SD-TMSR with reactor-grade Pu and TRU fissile materials is discussed. Additionally, the previously studied ^{233}U case is listed for comparison [26]. Figure 5 demonstrates the dynamics of the heavy metal refill rate during 60 EFPY of the SD-TMSR operation. The heavy metal refill rate was adjusted to maintain criticality and the total fuel mass almost constant[9] during reactor operation. In the ^{233}U case, the mean values of ^{233}U and ^{232}Th refill rate are 1.77 and 2.21 kg/d, respectively. Similarly, in the reactor-grade Pu case, the mean values of ^{233}U and Pu refill rate are 0.75 and 2.75 kg/d, respectively. For the TRU case, the mean values of ^{233}U and TRU refill rate are 0.90 and 2.0 kg/d, respectively.

Figures 6 and 7 demonstrate the evolution of important isotopes for the ^{233}U, Pu, and TRU cases respectively. For the ^{233}U case (Figure 6), the mass of Pa in the fuel salt is almost constant and reaches 17.8 kg at the end of the operation time. Additionally, the mass of minor actinides (MA) and Pu increases with time. The level of Pu in the fuel salt correlates with the mass of the MA; however,

[8] In the present work, the minor actinides (MA) include Np, Am, and Cm.

[9] The variation of the total fuel mass is less than 0.1%

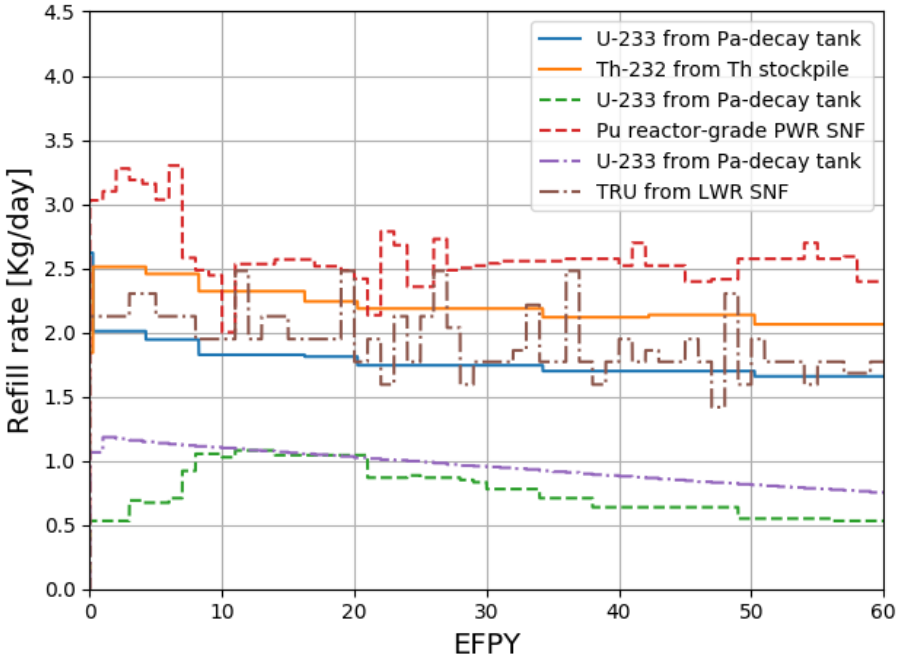

Figure 5: Dynamics of heavy metal refill rate during 60 EFPY of reactor operation. Solid lines for the ^{233}U case, dashed lines for the reactor-grade Pu case, and dotted lines for the TRU case.

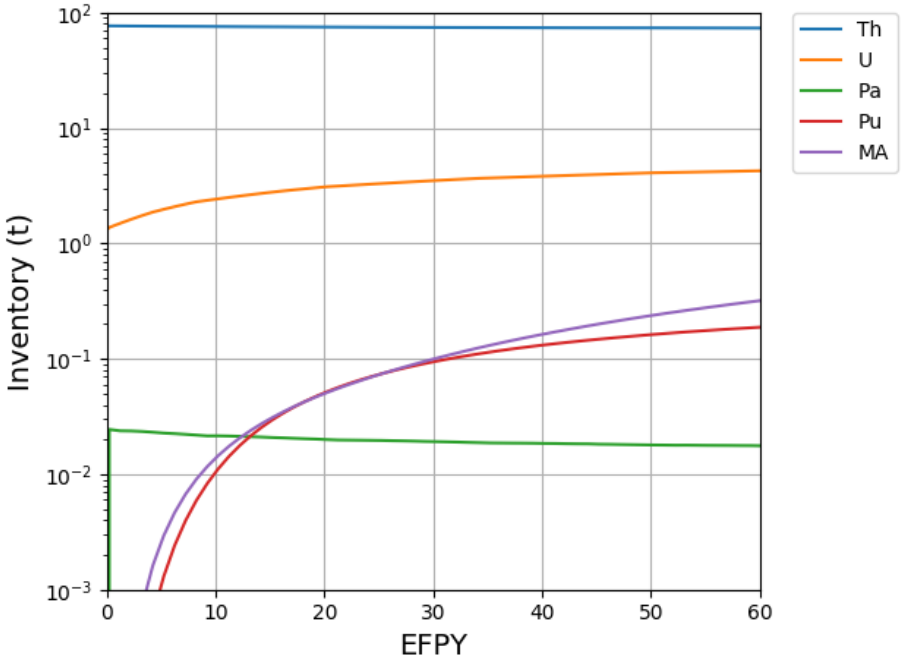

Figure 6: Evolution of the important nuclides inventories for the ^{233}U case (MA involves Np, Am, Cm) [26].

MA need more time to reach equilibrium than Pu. Uranium inventory increases during operation and reaches equilibrium after ≈ 27 years. Figure 6 shows that refueling the core with thorium helps maintain an almost constant inventory throughout the full operation time. For the Pu and TRU cases (Figure 7), the Pa extraction time was selected to be 30 s to avoid poisoning the core. Figure 7 shows that the mass of Pa in the fuel salt is relatively low when compared to Pa mass in the ^{233}U case (Figure 6). Major isotopes for all three cases reach the equilibrium state after ≈ 30 years (see Figure 6 and 7).

Figure 8 illustrates the variation of thorium inventory in the fuel salt for the ^{233}U, reactor-grade Pu, and TRU cases. The thorium inventory decreases in the ^{233}U case by only 3.2% at the End Of Life (EOL) when the thorium feed mechanism is applied. In contrast, thorium total mass decreases significantly in the Pu and TRU cases when the non-thorium feed mechanism is applied. Thus,

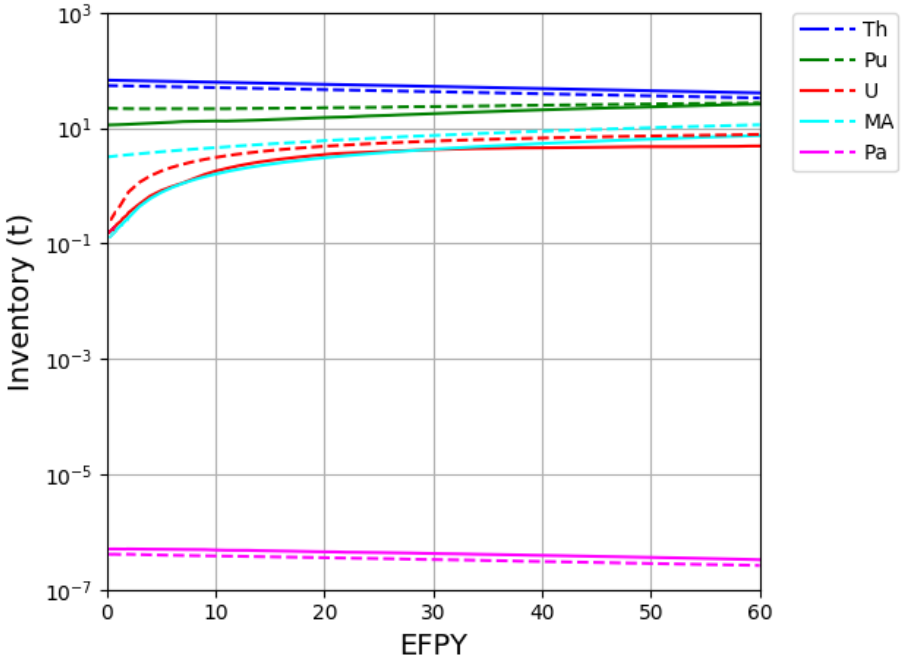

Figure 7: Evolution of the important nuclides inventories for the reactor-grade Pu case (solid lines) and for the TRU case (dashed lines).

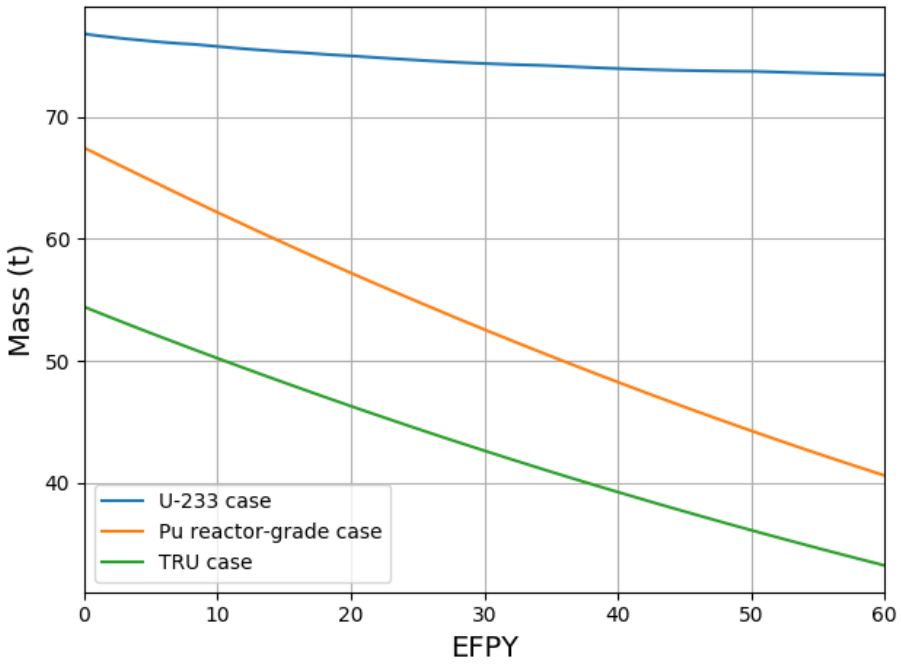

Figure 8: The variation of thorium mass in the fuel salt for the ^{233}U, reactor-grade Pu, and TRU cases.

thorium mass decreases by 39.21% and 37.96% for the reactor-grade Pu and TRU cases, respectively.

Figure 9 demonstrates the mass of ^{233}U in the fuel salt for the ^{233}U, reactor-grade Pu, and TRU cases. The mass of ^{233}U reaches equilibrium after $\approx$ 30 years; overall, the amount of ^{233}U is sufficient to maintain criticality in the three cases.

In the non-thorium feed mechanism, the SD-TMSR is continuously refueled by heavy metals (Pu and TRU) for criticality, which increases the Pu molar fraction (mole%) in the molten salt. According to literature, the limit of Pu solubility in the FLiBe salt is $\approx$ 4.0 mole% [31, 32]. Figure 10 represents the Pu fraction in the fuel salt (mole%) for the ^{233}U, reactor-grade Pu, and TRU cases, respectively. In the ^{233}U and reactor-grade Pu cases, the Pu fraction increases slightly but still below its solubility limit. On the other hand, the Pu fraction

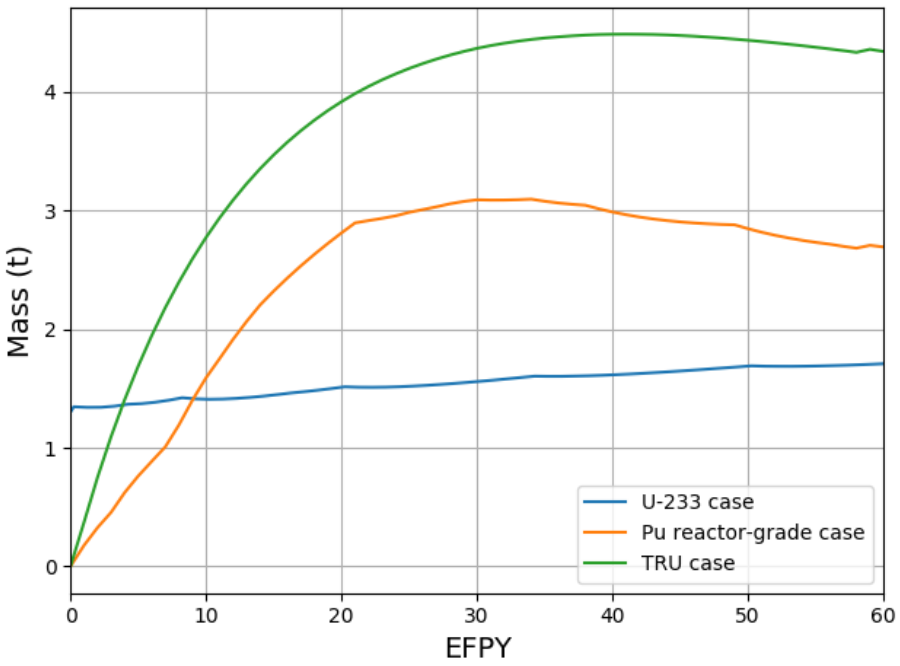

Figure 9: Mass of ^{233}U in the fuel salt for the ^{233}U, reactor-grade Pu, and TRU cases.

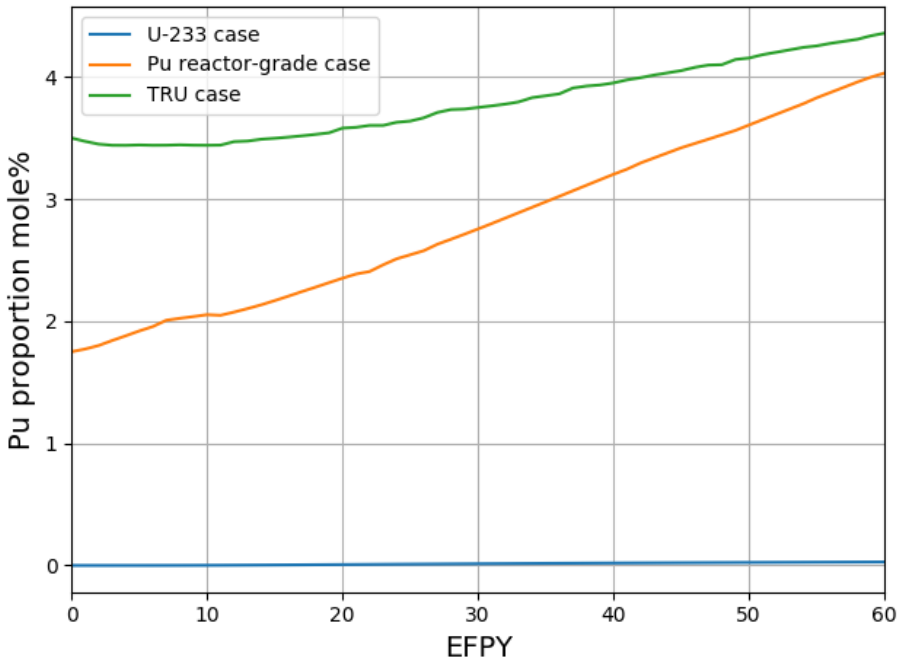

Figure 10: The Pu fraction in the fuel salt (mole%) for the ^{233}U, reactor-grade Pu, and TRU cases.

in the molten salt loaded by TRU increases during operation and reaches the Pu solubility limit after $\approx$ 40 years. This issue may be solved by increasing the reactor operation temperature or reducing the HM initial inventory [10].

Figure 11 demonstrates the net production of ^{233}U during operation for the ^{233}U, reactor-grade Pu, and TRU cases, respectively. For the TRU case, the net production of ^{233}U is almost zero. Although all produced ^{233}U is used to refuel the core, the reactor is subcritical after 40 years of operation (Figure 4). In the ^{233}U and reactor-grade Pu cases, the net production of ^{233}U increases with burnup and reaches about 1.77 t and 10 t at EOL, respectively. As shown in Figure 11, for the ^{233}U case, after 26 years the net production of ^{233}U reaches 1.3 t; this is sufficient to start up another SD-TMSR. Similarly, one can see that the same amount of ^{233}U (1.3 t) can be achieved after $\approx$ 4.5 years if we apply the non-thorium feed mechanism on the SD-TMSR that was initially loaded by

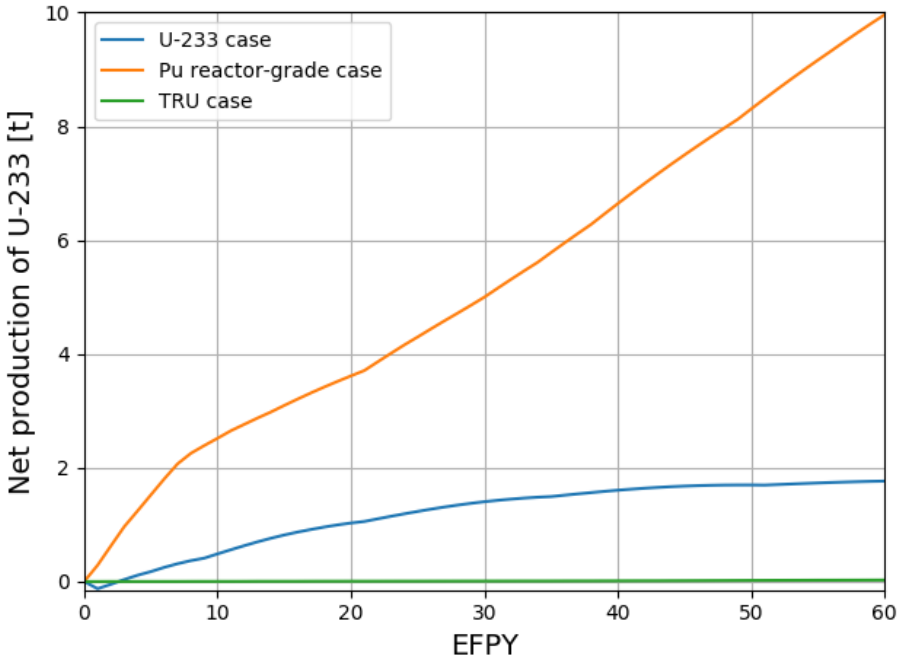

Figure 11: Net production of ^{233}U during the burnup period (60 EFPY) for the ^{233}U, reactor-grade Pu, and TRU cases.

reactor-grade Pu alternative to ^{233}U. In addition, Figure 11 shows that for the ^{233}U case the net production of ^{233}U during the first 455 days is negative; about 175.28 kg of ^{233}U must be added during this period. In conclusion, the thorium fuel cycle transition can be achieved by selecting the proper feed mechanism and initial fissile material. Specifically, applying the non-thorium feed mechanism on the SD-TMSR loaded by reactor-grade Pu allows the transition to the thorium fuel cycle after $\approx$ 4.5 years. Additionally, applying the thorium feed mechanism on the SD-TMSR loaded by ^{233}U allows the transition to the thorium fuel cycle after $\approx$ 26 years of operation. The comparison between the two feed mechanisms with different types of initial fuel is listed in Table 7.

Table 7: Comparison between the two feed mechanisms for the five different types of initial fuel.

Feed mechanism	LEU (19.79%)	Pu+enriched U (19.79wt.%)	reactor-grade Pu	TRU	^{233}U
Thorium feed mechanism	✗	✗	✗	✗	✓
Non-thorium feed mechanism	✗	✗	✓[a]	✓[b]	✗[c]

[a]Positive ^{233}U net production and critical configuration for 60 years of operation.
[b]Zero ^{233}U net production and critical configuration for 40 years of operation.
[c]Too large and increasing k_{eff} during lifetime.

5.4. Neutron spectrum

Figure 12 represents the neutron flux per unit lethargy for a full-core SD-TMSR model in the energy range from 10^{-8} to 10 MeV for the ^{233}U, reactor-grade Pu, and TRU cases at BOL and EOL. In the ^{233}U case, at the EOL, the neutron spectrum is harder than at BOL due to the accumulation of Pu and other strong thermal neutron absorbers in the fuel salt. For the reactor-grade Pu and TRU cases, during reactor operation, the fissile Pu is depleted and the ^{233}U becomes the major fissile isotope (see Figure 9); the neutron spectrum softens and becomes similar to the initial thermal spectrum of a ^{233}U fueled SD-TMSR.

5.5. Neutron flux

Figures 13 and 14 show the radial distribution of fast (energy range between 0.625 eV and 20 MeV) and thermal (energy range between 10^{-5} eV and 0.625 eV) neutron flux for three different initial fissile materials in the fuel salt (^{233}U, reactor-grade Pu, TRU) at startup and at equilibrium (after $\approx$ 30 years of operation). Actinides' evolution and poisonous fission product accumulation for various initial fissile compositions demonstrates the different effects on the SD-TMSR neutronics performance. For the ^{233}U case, the thermal neutron flux

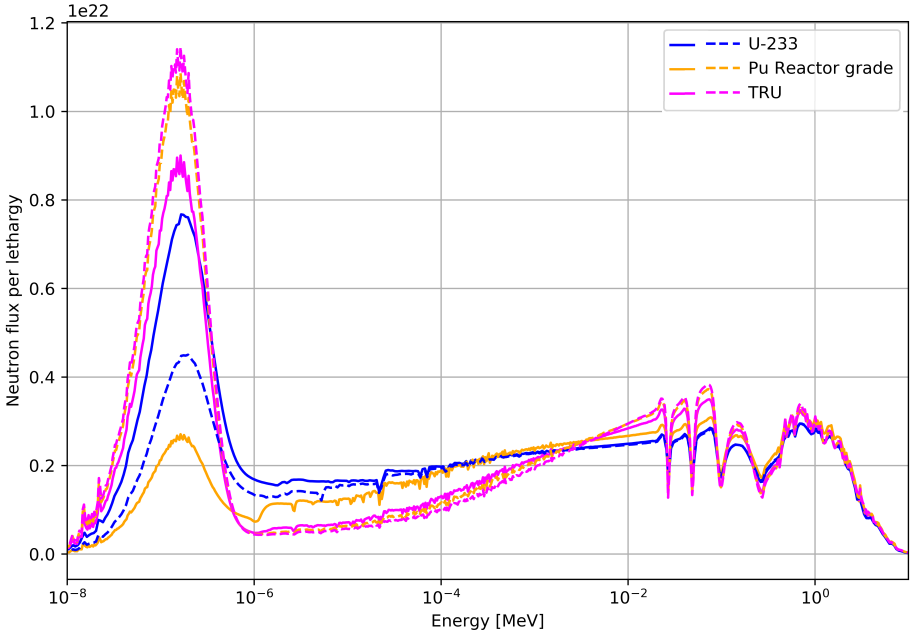

Figure 12: The neutron flux energy spectrum at BOL (solid lines) and EOL (dashed lines) for the ^{233}U, reactor-grade Pu, and TRU cases.

is suppressed at equilibrium because fissile ^{233}U in the core is being substituted with heavier fissile actinides: ^{235}U, ^{239}Pu, and ^{241}Pu. This agrees with results in literature [7, 26].

Opposite behavior is observed for the reactor-grade Pu and TRU cases. For these cases, the thermal neutron flux increases during operation while fast neutron flux decreases. Fissile Pu nuclides (generate relatively hard spectrum) from initial fuel salt composition are gradually substituted with ^{233}U (generates relatively soft spectrum), produced from fertile ^{232}Th. During reactor operation, ^{233}U becomes the primary fissile isotope, which softening the neutron spectrum of the reactor.

More changes in thermal neutron flux shape and magnitude for the ^{233}U case are observed in the inner core zone ($R \lesssim 150$) than in the outer core zone. In contrast, for the reactor-grade Pu and TRU cases, significant changes are observed for thermal neutron flux in the outer core zone and reflector.

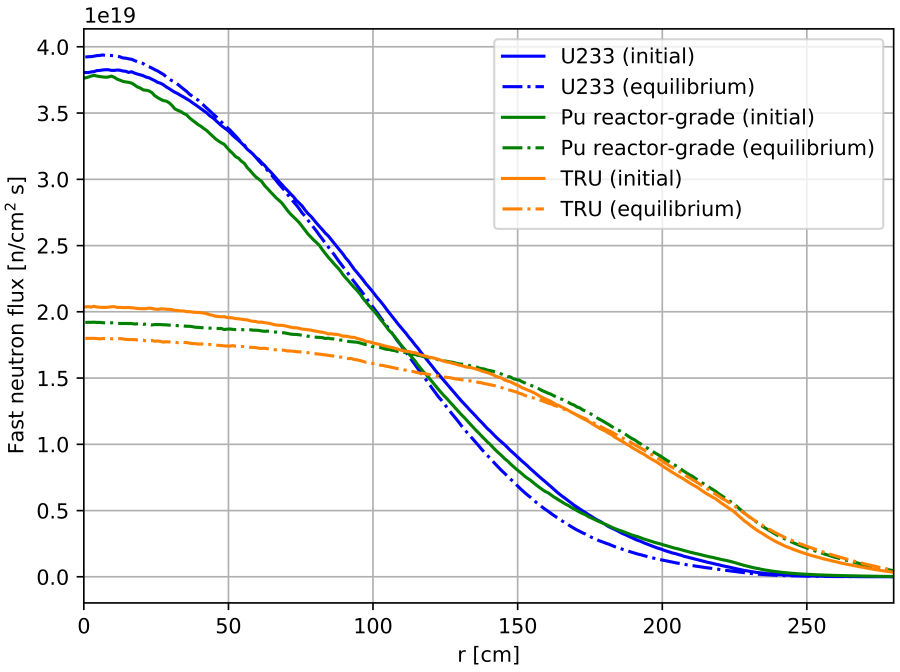

Figure 13: Radial fast neutron flux distribution for 3 different initial fuel salt compositions at startup and equilibrium (the fast flux confidence interval $\pm\sigma < 2.5\%$ for all cases).

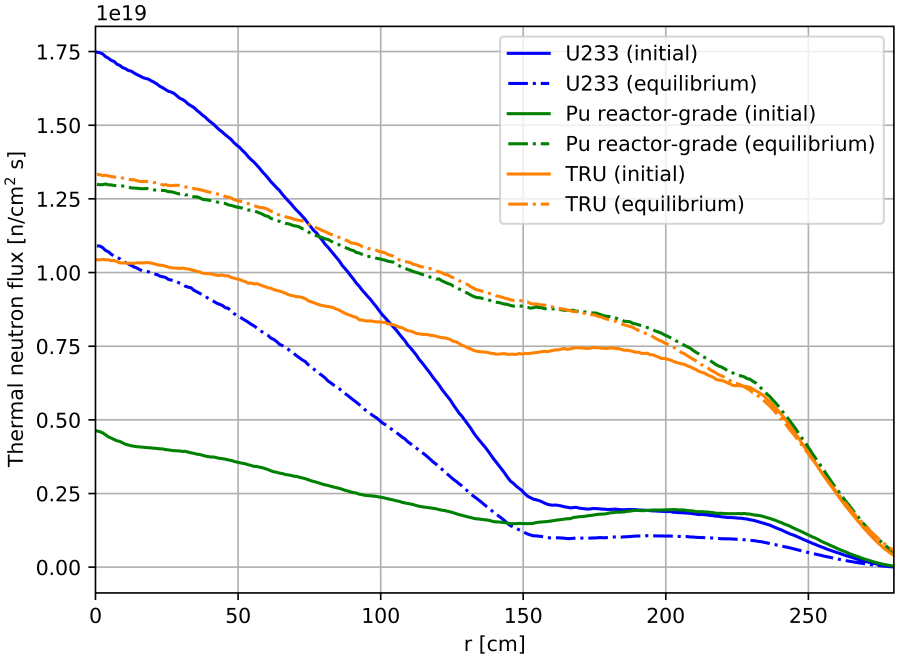

Figure 14: Radial thermal neutron flux distribution for 3 different initial fuel salt compositions at startup and equilibrium (the thermal flux confidence interval $\pm\sigma < 1.6\%$ for all cases).

Additionally, Figure 14 shows relatively large changes in thermal flux leakage from the core for the Pu and TRU cases. The SD-TMSR core design was optimized for ^{233}U [5]; thus, the core geometry (e.g., channels lattice pitch) must be re-optimized for another type of fuel to obtain better neutronics performance.

5.6. Temperature coefficient of reactivity

The temperature coefficient of reactivity quantifies reactivity changes due to temperature increase in the core and is calculated in this work as follows:

$$\alpha = \frac{k_{eff}(T_{i+1}) - k_{eff}(T_i)}{k_{eff}(T_{i+1})k_{eff}(T_i)(T_{i+1} - T_i)} \tag{2}$$

where

$$k_{eff} = \text{effective multiplication factor}$$

$$T_i = \text{fuel salt temperature in (900 K, 1000 K).}$$

Table 8 summarizes temperature coefficients calculated for three different initial fissile loads at startup and at equilibrium. By propagating the k_{eff} statistical error provided by SERPENT-2, uncertainty for each temperature coefficient is calculated using the following formula:

$$\delta\alpha = \left|\frac{1}{T_{i+1} - T_i}\right| \sqrt{\frac{\delta k_{eff}^2(T_{i+1})}{k_{eff}^4(T_{i+1})} + \frac{\delta k_{eff}^2(T_i)}{k_{eff}^4(T_i)}} \tag{3}$$

where

$$\delta k_{eff} = \text{statistical error for } k_{eff} \text{ from SERPENT-2 output.}$$

Other sources of uncertainty are neglected, such as cross section measurement error and approximations inherent in the density dependence on temperature.

When the fuel salt temperature increases, the density of the salt decreases, but at the same time, the total volume of fuel salt in the core remains constant because it is bounded by the vessel. When the graphite temperature increases, the density of graphite decreases, creating additional space for the salt. The cross section temperatures for the fuel and moderator were changed from 900 to 1000 K to determine the temperature coefficients. This work considered five different cases:

1. Fuel salt temperature (Doppler Effect) rising from 900 to 1000 K (first row in Table 8).

2. Fuel salt density decreasing from 3.3 to 3.233 g/cm^3 (density change caused by temperature increase from 900 to 1000 K).

3. Total fuel salt temperature (Doppler+density) rising from 900 to 1000 K.

4. Graphite temperature (Doppler Effect) rising from 900 to 1000 K.

5. Whole reactor temperature rising from 900 K to 1000 K.

In the first case, the fuel temperature change only impacts cross section temperature. In the second case, changes in the fuel temperature only impact density, and the third case takes into account both effects. The geometry for these three cases is unchanged because the fuel is a liquid. However, when the graphite blocks heat up, both the density and the geometry change due to the thermal expansion of solid graphite. The graphite linear thermal expansion is not a dominating factor [5], and herein we focus only on the Doppler Effect for the moderator temperature coefficient.

The Fuel Temperature Coefficient (FTC) is negative for all considered fuel compositions due to thermal Doppler broadening of the resonance capture cross

Table 8: Temperature coefficients of reactivity for 3 different initial fuel salt compositions at startup and equilibrium. Confidence interval $\pm\sigma$ for all coefficients is between 0.11 and 0.16 pcm/K).

Reactivity coefficient (pcm/K)	Startup fissile material					
	^{233}U		Pu		TRU	
	Initial	Equil.	Initial	Equil.	Initial	Equil.
Fuel salt temperature	−4.96	−5.26	−4.99	−3.12	−3.23	−1.97
Fuel salt density	+1.49	+2.34	+1.54	−1.58	−0.37	−1.62
Total salt fuel	−3.77	−2.83	−3.22	−4.23	−3.25	−3.69
Graphite temperature	+1.45	+0.45	−2.68	−1.37	−1.44	−1.14
Total core	−1.77	−2.59	−6.54	−5.06	−4.79	−4.76

sections in the thorium. For the ^{233}U case, the FTC decreases in magnitude by 25% due to neutron spectrum hardening during the reactor operation. For reactor-grade Pu and TRU cases, the FTC increases in magnitude at equilibrium, by 31% and 14%, respectively. Spectrum softening for these fueling cases positively affects the FTC magnitude, and this effect seems to be proportional to the spectrum shift.

The Moderator Temperature Coefficient (MTC) for the ^{233}U case is positive and decreases during reactor operation because of spectrum hardening with fuel depletion. For other cases, the MTC is negative and also decreases in magnitude during reactor operation. Finally, the total temperature coefficient of reactivity is strongly negative for all considered scenarios but decreases in magnitude during reactor operation due to spectral shift. Notably, the total temperature coefficient is the most negative for the reactor-grade Pu case at startup, which has the hardest neutron spectrum (Figure 12). These coefficients agree with earlier estimates for the SD-TMSR [5, 26] and MSBR [7, 33, 23].

Even after 30 years of operation, the total temperature coefficient of reactivity remains relatively large and negative (in the range between -2.59 and -5.06 pcm/K) compared to the conventional PWR, which has temperature coefficient of about $-1.71\ pcm/^{\circ}F \approx -3.08\ pcm/K$ [34], and allows excellent reactor stability and control. The additional analysis must be performed taking graphite moderator density change and linear thermal expansion into account, but material properties for the SD-TMSR graphite are not available in published literature. Relatively well-studied reactor graphite (e.g., AXQ graphite [23]) can be considered as a candidate for the SD-TMSR concept.

5.7. Six factor analysis

The effective multiplication factor can be expressed as follows:

$$k_{eff} = \eta f p \epsilon P_f P_t \tag{4}$$

where

$$\eta = \text{thermal fission factor}$$

$$f = \text{thermal utilization factor}$$

$$p = \text{resonance escape probability}$$

$$\epsilon = \text{fast fission factor}$$

$$P_f = \text{fast non-leakage probability}$$

$$P_t = \text{thermal non-leakage probability.}$$

Table 9 summarizes the six factors for 3 different initial fuel salt compositions at startup and equilibrium. By using SERPENT-2 built-in online reprocessing capabilities, all six factors are calculated at the beginning of the operation and after 30 years of operation. Neutron population and number of active/inactive cycles were selected to obtain k_{eff} statistical uncertainty less than 12 pcm. The fast and thermal non-leakage probabilities remain constant regardless of initial fissile material and neutron spectrum shift during operation. The thermal utilization factor (f) remains almost constant during operation for the ^{233}U and TRU cases but considerably declines for the Pu case due to significant neutron spectrum softening.

Table 9: Six factors for the SD-TMSR model for 3 different initial fuel salt compositions at startup and equilibrium.

Factor	Startup fissile material					
	^{233}U		Pu		TRU	
	Initial	Equil	Initial	Equil	Initial	Equil
η	1.26	1.40	1.66	1.44	1.59	1.31
f	0.97	0.98	0.96	0.76	0.80	0.75
p	0.54	0.43	0.26	0.16	0.17	0.15
ϵ	1.49	1.67	2.45	5.87	4.83	6.81
P_f	0.99	0.99	0.99	0.99	0.99	0.99
P_t	1.00	1.00	1.00	1.00	1.00	1.00

In contrast, the neutron reproduction factor (η), resonance escape probability (p), and fast fission factor (ϵ) differ notably between the initial and equilibrium state for all three initial fissile materials. ϵ is much larger at startup for the Pu and TRU cases because these initial fissile materials provide a much harder neutron spectrum than ^{233}U, and ϵ grows throughout the core's lifetime. Conversely, p decreases during reactor operation. The thermal fission factor (η) increases during reactor operation for the ^{233}U as initial fuel due to the accumulation of fissile plutonium isotopes, which produce more neutrons per fission (ν). The other two scenarios demonstrate opposite behavior: plutonium isotopes with large ν are gradually substituted with ^{233}U, which has a lower ν [35]. This six factors' evolution agrees with previously determined evolution parameters for a similar single-fluid double-zone MSBR [26, 7, 36].

6. Conclusion

Five different types of initial fissile loadings have been studied for transitioning to the thorium fuel cycle in the Single-fluid Double-zone Thorium-based Molten Salt Reactor (SD-TMSR). We adopted two different feed mechanisms: thorium feed mechanism and non-thorium feed mechanism. Lifetime-long depletion for the whole-core SD-TMSR model was performed with reactor-grade Pu, TRU, and ^{233}U as initial fissile materials. Additionally, the dynamics of the effective multiplication factor k_{eff}, major isotopes mass, neutron energy spectrum, and essential safety parameters have been investigated.

Results demonstrate that continuous flow of reactor-grade Pu allows the transition to the thorium fuel cycle in a relatively short time ($\approx$ 4.5 years) compared to 26 years for Th/^{233}U startup fuel. Meanwhile, using TRU as initial fissile materials shows the possibility of operating the SD-TMSR for an extended time ($\approx$ 40 years) without any external feed of ^{233}U. Notably, the Pu molar fraction (mole%) in fuel salt was calculated and found to be below the solubility limit.

The neutron energy spectrum shift during the reactor operation for the Pu

and TRU cases is different from the ^{233}U fueling scenario. The spectrum hardens for the ^{233}U initial fissile isotope during operation, but softens for the Pu and TRU cases. Notably, the most significant neutron energy spectrum shift was obtained for reactor-grade Pu startup loading.

We compared the operational and safety parameters of the SD-TMSR for all three startup fuels at both initial and equilibrium states. The total temperature coefficient of reactivity is negative and relatively large in all cases. For the TRU case, the coefficient remained almost constant during operation: -4.79 ± 0.12 pcm/K and -4.76 ± 0.11 pcm/K for the initial and equilibrium states, respectively. For reactor-grade Pu, the coefficient absolute value decreased from -6.54 ± 0.16 pcm/K to -4.79 ± 0.12 during 60 years of operation. Finally, the six factors evolution during the operation were calculated for all three cases, and these parameters can be used to design the reactivity control system of the SD-TMSR.

7. Future work

The authors intend to verify obtained results using another tool: batch-wise code SaltProc [37, 38]. In further simulations, we intend to take into account the delayed neutron precursor drift. The SD-TMSR reactivity control system has not been introduced in the literature yet. Thus, the control rods design and configuration might be suggested in the nearest future.

An additional area to explore is the accident safety analysis which requires high-fidelity multi-physics model of the SD-TMSR with the coupled neutronics/thermal-hydraulics software, Moltres [39]. The full-core SERPENT-2 model of the SD-TMSR and equilibrium fuel salt compositions, obtained in this work, would be employed to generate problem-oriented nuclear data libraries for Moltres. The ultimate goal of this effort is to develop a fast-running computational model for studying the dynamics behavior of generic MSRs, performing safety analysis for different accident scenarios and optimizing design of various reactor concepts.

8. Declaration of Competing Interest

The authors declare that they have no known competing financial interests or personal relationships that could have appeared to influence the work reported in this paper.

9. Acknowledgments

Osama Ashraf would like to thank the Egyptian Ministry of Higher Education (MoHE), as well as MEPhI's Competitiveness Program for providing financial support for this research. The facility and tools needed to conduct this work were supported by MEPhI.

The authors contributed to this work as described below.

Osama Ashraf conceived and designed the simulations, wrote the paper, prepared figures and/or tables, performed the computation work, and reviewed drafts of the paper.

Andrei Rykhlevskii conceived and designed the simulations, wrote the paper, prepared figures and/or tables, performed the computation work, and reviewed drafts of the paper. Andrei Rykhlevskii is supported by DOE ARPA-E MEITNER program award DE-AR0000983.

G. V. Tikhomirov directed and supervised the work, conceived and designed the simulations and reviewed drafts of the paper. Prof. Tikhomirov is supported by Rosatom, he is Deputy Director of the Institute of Nuclear Physics and Engineering MEPhI. Board member of Nuclear society of Russia.

Kathryn D. Huff supervised the work, conceived and contributed to conception of the simulations, and reviewed drafts of the paper. Prof. Huff is supported by the Nuclear Regulatory Commission Faculty Development Program, the National Center for Supercomputing Applications, the NNSA Office of Defense Nuclear Nonproliferation R&D through the Consortium for Verification Technologies and the Consortium for Nonproliferation Enabling Capabilities, the International Institute for Carbon Neutral Energy Research (WPI-I2CNER), sponsored by

the Japanese Ministry of Education, Culture, Sports, Science and Technology, and DOE ARPA-E MEITNER program award DE-AR0000983.

This research is part of the Blue Waters sustained-petascale computing project, which is supported by the National Science Foundation (awards OCI-0725070 and ACI-1238993) and the state of Illinois. Blue Waters is a joint effort of the University of Illinois at Urbana-Champaign and its National Center for Supercomputing Applications

References

[1] DOE, US, A technology roadmap for generation iv nuclear energy systems (2002) 48–52.

[2] D. D. Siemer, Why the molten salt fast reactor (msfr) is the best gen iv reactor, Energy Science & Engineering 3 (2) (2015) 83–97.

[3] M. Rosenthal, P. Kasten, R. Briggs, Molten-salt reactorshistory, status, and potential, Nuclear Applications and Technology 8 (2) (1970) 107–117.

[4] I. Pioro, Handbook of generation IV nuclear reactors, Woodhead Publishing, 2016.

[5] G. C. Li, P. Cong, C. G. Yu, Y. Zou, J. Y. Sun, J. G. Chen, H. J. Xu, Optimization of Th-U fuel breeding based on a single-fluid double-zone thorium molten salt reactor, Progress in Nuclear Energy 108 (2018) 144–151. doi:10.1016/j.pnucene.2018.04.017.
URL http://www.sciencedirect.com/science/article/pii/S0149197018300970

[6] A. Nuttin, D. Heuer, A. Billebaud, R. Brissot, C. Le Brun, E. Liatard, J.-M. Loiseaux, L. Mathieu, O. Meplan, E. Merle-Lucotte, et al., Potential of thorium molten salt reactorsdetailed calculations and concept evolution with a view to large scale energy production, Progress in nuclear energy 46 (1) (2005) 77–99.

[7] A. Rykhlevskii, J. W. Bae, K. D. Huff, Modeling and simulation of online reprocessing in the thorium-fueled molten salt breeder reactor, Annals of Nuclear Energy 128 (2019) 366–379. doi:10.1016/j.anucene.2019.01.030.

[8] E. Merle-Lucotte, D. Heuer, C. Le Brun, J. Loiseaux, Scenarios for a worldwide deployment of nuclear energy production.

[9] B. R. Betzler, J. J. Powers, A. Worrall, Modeling and simulation of the start-up of a thorium-based molten salt reactor, in: Proc. Int. Conf. PHYSOR, 2016.

[10] C. Zou, C. Cai, C. Yu, J. Wu, J. Chen, Transition to thorium fuel cycle for tmsr, Nuclear Engineering and Design 330 (2018) 420–428.

[11] C. Zou, G. Zhu, C. Yu, Y. Zou, J. Chen, Preliminary study on trus utilization in a small modular th-based molten salt reactor (smtmsr), Nuclear Engineering and Design 339 (2018) 75–82.

[12] D. Heuer, E. Merle-Lucotte, M. Allibert, M. Brovchenko, V. Ghetta, P. Rubiolo, Towards the thorium fuel cycle with molten salt fast reactors, Annals of Nuclear Energy 64 (2014) 421–429.

[13] O. Ashraf, A. Smirnov, G. Tikhomirov, Modeling and criticality calculation of the molten salt fast reactor using serpent code, in: Journal of Physics: Conference Series, Vol. 1189, IOP Publishing, 2019, p. 012007.

[14] O. Ashraf, A. Smirnov, G. Tikhomirov, Nuclear fuel optimization for molten salt fast reactor, in: Journal of Physics: Conference Series, Vol. 1133, IOP Publishing, 2018, p. 012026. doi:doi:10.1088/1742-6596/1133/1/012026.

[15] A. Rykhlevskii, B. R. Betzler, A. Worrall, K. D. Huff, Fuel Cycle Performance of Fast Spectrum Molten Salt Reactor Designs, in: Proceedings of Mathematics and Computation 2019, American Nuclear Society, Portland, OR, 2019.

[16] B. R. Betzler, A. Rykhlevskii, A. Worrall, K. Huff, Impacts of Fast-Spectrum Molten Salt Reactor Characteristics on Fuel Cycle Performance, Tech. rep., Oak Ridge National Lab.(ORNL), Oak Ridge, TN (United States) (2019).

[17] C. Fiorina, M. Aufiero, A. Cammi, F. Franceschini, J. Krepel, L. Luzzi, K. Mikityuk, M. E. Ricotti, Investigation of the msfr core physics and fuel cycle characteristics, Progress in Nuclear Energy 68 (2013) 153–168.

[18] C. de Saint Jean, M. Delpech, J. Tommasi, G. Youinou, P. Bourdot, Scénarios cne: réacteurs classiques, caractérisation à l'équilibre, rapport CEA DER/SPRC/LEDC/99-448.

[19] J. Leppänen, M. Pusa, T. Viitanen, V. Valtavirta, T. Kaltiaisenaho, The serpent monte carlo code: Status, development and applications in 2013, in: SNA+ MC 2013-Joint International Conference on Supercomputing in Nuclear Applications+ Monte Carlo, EDP Sciences, 2014, p. 06021.

[20] M. Jiang, H. Xu, Z. Dai, Advanced fission energy program-tmsr nuclear energy system, Bull. Chin. Acad. Sci 27 (3) (2012) 366–374.

[21] X. Li, X. Cai, D. Jiang, Y. Ma, J. Huang, C. Zou, C. Yu, J. Han, J. Chen, Analysis of thorium and uranium based nuclear fuel options in fluoride salt-cooled high-temperature reactor, Progress in Nuclear Energy 78 (2015) 285–290.

[22] G. Li, Y. Zou, C. Yu, et al., Model optimization and analysis of th–u breeding based on msfr, Nucl. Tech 40 (2017) 020603–020603.

[23] R. C. Robertson, Conceptual Design Study of a Single-Fluid Molten-Salt Breeder Reactor., Tech. Rep. ORNL–4541, comp.; Oak Ridge National Laboratory, Tenn. (Jan. 1971).
URL http://www.osti.gov/scitech/biblio/4030941

[24] O. Ashraf, G. Tikhomirov, Preliminary study on the online reprocessing and refueling scheme for sd-tms reactor, in: Journal of Physics: Conference Series, IOP Publishing, 2019. doi:doi:.

[25] J. C. Marka, Explosive properties of reactor-grade plutonium, Science & Global Security 4 (1) (1993) 111–128.

[26] O. Ashraf, A. Rykhlevskii, G. Tikhomirov, K. D. Huff, Whole core analysis of the single-fluid double-zone torium molten salt reactor (sd-tmsr), Annals of Nuclear Energy.
URL https://doi.org/10.1016/j.anucene.2019.107115

[27] N. OECD, Probabilistic safety assessment in nuclear power plant management: a report by a group of experts of the nea committee on the safety of nuclear installations, june 1989, 112 (1989).

[28] J. Serp, M. Allibert, O. Beneš, S. Delpech, O. Feynberg, V. Ghetta, D. Heuer, D. Holcomb, V. Ignatiev, J. L. Kloosterman, et al., The molten salt reactor (msr) in generation iv: overview and perspectives, Progress in Nuclear Energy 77 (2014) 308–319.

[29] M. Aufiero, A. Cammi, C. Fiorina, J. Leppänen, L. Luzzi, M. E. Ricotti, An extended version of the serpent-2 code to investigate fuel burn-up and core material evolution of the molten salt fast reactor, Journal of Nuclear Materials 441 (1-3) (2013) 473–486.

[30] A. Isotalo, M. Pusa, Improving the accuracy of the chebyshev rational approximation method using substeps, Nuclear Science and Engineering 183 (1) (2016) 65–77.

[31] V. Ignatiev, O. Feynberg, A. Merzlyakov, A. Surenkov, A. Zagnitko, V. Afonichkin, A. Bovet, V. Khokhlov, V. Subbotin, R. Fazilov, et al., Progress in development of mosart concept with th support, in: Proceedings of ICAPP, Vol. 12394, 2012.

[32] D. Sood, P. Iyer, R. Prasad, V. Vaidya, K. Roy, V. Venugopal, Z. Singh, M. Ramaniah, Plutonium trifluoride as a fuel for molten salt reactors-solubility studies, Nuclear technology 27 (3) (1975) 411–415.

[33] A. Rykhlevskii, A. Lindsay, K. D. Huff, Full-core analysis of thorium-fueled Molten Salt Breeder Reactor using the SERPENT 2 Monte Carlo code, in: Transactions of the American Nuclear Society, American Nuclear Society, Washington, DC, United States, 2017.

[34] B. Forget, K. Smith, S. Kumar, M. Rathbun, J. Liang, Integral Full Core Multi-Physics PWR Benchmark with Measured Data, Tech. rep., Massachusetts Institute of Technology (2018).

[35] N. G. Sjöstrand, J. S. Story, Cross sections and neutron yields for U-233, U-235 and Pu-239 at 2200 m/sec, Tech. rep., AB Atomenergi (1960).

[36] J. Park, Y. Jeong, H. C. Lee, D. Lee, Whole core analysis of molten salt breeder reactor with online fuel reprocessing, International Journal of Energy Research 39 (12) (2015) 1673–1680. doi:10.1002/er.3371.
URL http://doi.wiley.com/10.1002/er.3371

[37] A. Rykhlevskii, J. W. Bae, K. Huff, arfc/saltproc: Code for online reprocessing simulation of molten salt reactor with external depletion solver SERPENT, Zenododoi:10.5281/zenodo.1196455.
URL https://zenodo.org/record/1196455#.WqrE_BPwaA0

[38] A. Rykhlevskii, K. Huff, Milestone 2.1 Report: Demonstration of SaltProc, Milestone Report UIUC-ARFC-2019-04 DOI: 10.5281/zenodo.3355649, University of Illinois at Urbana-Champaign, Urbana, IL (Jun. 2019). doi:10.5281/zenodo.3355649.
URL https://zenodo.org/record/3355649#.XZuyEEFKjdI

[39] A. Lindsay, G. Ridley, A. Rykhlevskii, K. Huff, Introduction to Moltres: An application for simulation of Molten Salt Reactors, Annals of Nuclear Energy 114 (2018) 530–540. doi:10.1016/j.anucene.2017.12.025.

Appendix A. Feed rates for all cases

Table A.1: The refueling table for Th/^{233}U case.

Material	**Feed rate**	**Feed constant*** λ_e $[s^{-1}]$
^{232}Th	1.842 [kg/day], first 90 [d]	1.500E-09
	2.511 [kg/day], from 90 to 1550 [d]	2.045E-09
	2.456 [kg/day], from 1550 to 3010 [d]	2.000E-09
	2.321 [kg/day], from 3010 to 5930 [d]	1.890E-09
	2.241 [kg/day], from 5930 to 7390 [d]	1.825E-09
	2.186 [kg/day], from 7390 to 12500 [d]	1.780E-09
	2.118 [kg/day], from 12500 to 15420 [d]	1.725E-09
	2.136 [kg/day], from 15420 to 18340 [d]	1.740E-09
	2.063 [kg/day], from 18340 to 21900 [d]	1.680E-09
^{233}U	2.619 [kg/day], first 90 [d]	6.400E-09
	2.009 [kg/day], form 90 to 1550 [d]	4.910E-09
	1.944 [kg/day], from 1550 to 3010 [d]	4.750E-09
	1.826 [kg/day], from 3010 to 5930 [d]	4.460E-09
	1.811 [kg/day], from 5930 to 7390[d]	4.425E-09
	1.744 [kg/day], from 7390 to 12500 [d]	4.260E-09
	1.699 [kg/day], from 12500 to 18340 [d]	4.150E-09
	1.657 [kg/day], from 18340 to 21900 [d]	4.050E-09

* Feed constant is the mass fraction of fertile or fissile nuclides (^{232}Th or ^{233}U) transferred from the external storage to the core per second.

Table A.2: The refueling table for reactor-grade Pu case.

Material	**Feed rate**	**Feed constant λ_e** $[s^{-1}]$
Pu	3.028 [kg/day], first 365 [d]	1.71E-08
	3.099 [kg/day], from 365 to 730 [d]	1.75E-08
	3.276 [kg/day], from 730 to 1095 [d]	1.85E-08
	3.188 [kg/day], from 1095 to 1460 [d]	1.80E-08
	3.158 [kg/day], from 1460 to 1825 [d]	1.78E-08
	3.034 [kg/day], from 1825 to 2190 [d]	1.71E-08
	3.299 [kg/day], from 2190 to 2555 [d]	1.86E-08
	2.581 [kg/day], from 2555 to 2920 [d]	1.46E-08
	2.484 [kg/day], from 2920 to 3285 [d]	1.40E-08
	2.444 [kg/day], from 3285 to 3650 [d]	1.38E-08
	2 [kg/day], from 3650 to 4015 [d]	1.13E-08
	2.532 [kg/day], from 4015 to 5110 [d]	1.43E-08
	2.568 [kg/day], from 5110 to 6205 [d]	1.45E-08
	2.515 [kg/day], from 6205 to 6935 [d]	1.42E-08
	2.483 [kg/day], from 6935 to 7300 [d]	1.40E-08
	2.417 [kg/day], from 7300 to 7665 [d]	1.37E-08
	2.134 [kg/day], from 7665 to 8030 [d]	1.21E-08
	2.786 [kg/day], from 8030 to 8395 [d]	1.57E-08
	2.679 [kg/day], from 8395 to 8760 [d]	1.51E-08
	2.355 [kg/day], from 8760 to 9490 [d]	1.33E-08
	2.727 [kg/day], from 9490 to 9855 [d]	1.54E-08
	2.484 [kg/day], from 9855 to 10220 [d]	1.40E-08
	2.502 [kg/day], from 10220 to 10585 [d]	1.41E-08
	2.520 [kg/day], from 10585 to 10950 [d]	1.42E-08
	2.538 [kg/day], from 10950 to 11315 [d]	1.43E-08
	2.555 [kg/day], from 11315 to 13140 [d]	1.44E-08
	2.573 [kg/day], from 13140 to 14600 [d]	1.45E-08

	2.520 [kg/day], from 14600 to 16425 [d]	1.42E-08
	2.396 [kg/day], from 16425 to 17155 [d]	1.35E-08
	2.414 [kg/day], from 17155 to 17885 [d]	1.36E-08
	2.573 [kg/day], from 17885 to 19710 [d]	1.45E-08
	2.697 [kg/day], from 19710 to 20075 [d]	1.52E-08
	2.573 [kg/day], from 20075 to 21170 [d]	1.45E-08
	2.39 [kg/day], from 21170 to 21900 [d]	1.35E-08
^{233}U	0.531 [kg/day], from 365 to 1095 [d]	3.00E-09
	0.690 [kg/day], form 1095 to 1460 [d]	3.90E-09
	0.673 [kg/day], from 1460 to 2190 [d]	3.80E-09
	0.708 [kg/day], from 2190 to 2555 [d]	4.00E-09
	0.921 [kg/day], from 2555 to 2920 [d]	5.20E-09
	1.053 [kg/day], from 2920 to 3650 [d]	5.95E-09
	1.027 [kg/day], from 3650 to 4015 [d]	5.80E-09
	1.080 [kg/day], from 4015 to 5110 [d]	6.10E-09
	1.043 [kg/day], from 5110 to 7665 [d]	5.89E-09
	0.867 [kg/day], from 7665 to 8760 [d]	4.90E-09
	0.885 [kg/day], from 8760 to 9125 [d]	5.00E-09
	0.867 [kg/day], from 9125 to 10220 [d]	4.90E-09
	0.850 [kg/day], from 10220 to 10585 [d]	4.80E-09
	0.832 [kg/day], from 10585 to 10950 [d]	4.70E-09
	0.779 [kg/day], from 10950 to 12410 [d]	4.40E-09
	0.708 [kg/day], from 12410 to 13870 [d]	4.00E-09
	0.637 [kg/day], from 13870 to 17885 [d]	3.60E-09
	0.549 [kg/day], from 17885 to 20440 [d]	3.10E-09
	0.531 [kg/day], from 20440 to 21900 [d]	3.00E-09

Table A.3: The refueling table for TRU case.

Material	**Feed rate**	**Feed constant λ_e** $[s^{-1}]$
TRU	2.125 [kg/day], first 365 to 1095 [d]	1.20E-08
	2.302 [kg/day], from 1095 to 1825 [d]	1.30E-08
	2.125 [kg/day], from 1825 to 2920 [d]	1.20E-08
	1.9488 [kg/day], from 2920 to 4015 [d]	1.10E-08
	2.479 [kg/day], from 4015 to 4380 [d]	1.40E-08
	1.948 [kg/day], from 4380 to 4745 [d]	1.10E-08
	2.125 [kg/day], from 4745 to 5110 [d]	1.20E-08
	1.948 [kg/day], from 5110 to 6935 [d]	1.10E-08
	2.479 [kg/day], from 6935 to 7300 [d]	1.40E-08
	1.771 [kg/day], from 7300 to 7665 [d]	1.00E-08
	1.948 [kg/day], from 7665 to 8030 [d]	1.10E-08
	1.594 [kg/day], from 8030 to 8395 [d]	0.90E-08
	2.125 [kg/day], from 8395 to 8760 [d]	1.20E-08
	1.771 [kg/day], from 8760 to 9125 [d]	1.00E-08
	2.125 [kg/day], from 9125 to 9490 [d]	1.20E-08
	2.479 [kg/day], from 9490 to 9855 [d]	1.4E-08
	2.036 [kg/day], from 9855 to 10220 [d]	1.15E-08
	1.594 [kg/day], from 10220 to 10585 [d]	0.90E-08
	1.771 [kg/day], from 10585 to 11680 [d]	1.00E-08
	1.859 [kg/day], from 11680 to 12045 [d]	1.05E-08
	2.214 [kg/day], from 12045 to 12410 [d]	1.25E-08
	1.771 [kg/day], from 12410 to 13140 [d]	1.00E-08
	2.479 [kg/day], from 13140 to 13505 [d]	1.40E-08
	1.771 [kg/day], from 13505 to 13870 [d]	1.00E-08
	1.594 [kg/day], from 13870 to 14235 [d]	0.90E-08
	1.771 [kg/day], from 14235 to 14600 [d]	1.00E-08
	1.948 [kg/day], from 14600 to 14965 [d]	1.10E-08

	1.771 [kg/day], from 14965 to 17155 [d]	1.00E-08
	1.416 [kg/day], from 17155 to 17520 [d]	0.80E-08
	2.302 [kg/day], from 17520 to 17885 [d]	1.30E-08
	1.594 [kg/day], from 17885 to 18250 [d]	0.90E-08
	1.771 [kg/day], from 18250 to 20440 [d]	1.00E-08
	1.594 [kg/day], from 20440 to 21170 [d]	0.90E-08
	1.771 [kg/day], from 21170 to 21900 [d]	1.00E-08
^{233}U	1.066 [kg/day], first 365 [d]	6.02E-09
	1.177 [kg/day], form 365 to 1095 [d]	6.65E-09
	1.160 [kg/day], from 1095 to 1460 [d]	6.55E-09
	1.142 [kg/day], from 1460 to 2190 [d]	6.45E-09
	1.124 [kg/day], from 2190 to 2920 [d]	6.35E-09
	1.107 [kg/day], from 2920 to 4015 [d]	6.25E-09
	1.089 [kg/day], from 4015 to 4745 [d]	6.15E-09
	1.071 [kg/day], from 4745 to 5475 [d]	6.05E-09
	1.053 [kg/day], from 5475 to 6570 [d]	5.95E-09
	1.036 [kg/day], from 6570 to 7300 [d]	5.85E-09
	1.018 [kg/day], from 7300 to 8030 [d]	5.75E-09
	1 [kg/day], from 8030 to 9125 [d]	5.65E-09
	0.983 [kg/day], from 9125 to 9855 [d]	5.55E-09
	0.965 [kg/day], from 9855 to 10950 [d]	5.45E-09
	0.947 [kg/day], from 10950 to 12045 [d]	5.35E-09
	0.929 [kg/day], from 12045 to 12775 [d]	5.25E-09
	0.912 [kg/day], from 12775 to 13505 [d]	5.15E-09
	0.894 [kg/day], from 13505 to 14600 [d]	5.05E-09
	0.876 [kg/day], from 14600 to 15330 [d]	4.95E-09
	0.859 [kg/day], from 15330 to 16425 [d]	4.85E-09
	0.841 [kg/day], from 16425 to 17155 [d]	4.75E-09
	0.823 [kg/day], from 17155 to 18250 [d]	4.65E-09
	0.805 [kg/day], from 18250 to 19345 [d]	4.65E-09

	0.788 [kg/day], from 19345 to 20440 [d]	4.45E-09
	0.770 [kg/day], from 20440 to 21535 [d]	4.35E-09
	0.752 [kg/day], from 20440 to 21900 [d]	4.25E-09